HHS Public Access

Author manuscript

Magn Reson Med. Author manuscript; available in PMC 2017 June 01.

Published in final edited form as:

Magn Reson Med. 2016 June ; 75(6): 2278–2285. doi:10.1002/mrm.25788.

Real-time distortion correction of spiral and echo planar images using the gradient system impulse response function

Adrienne E Campbell-Washburn[*], **Hui Xue**, **Robert J Lederman**, **Anthony Z Faranesh**, and **Michael S Hansen**

Pulmonary and Cardiovascular Branch, Division of Intramural Research, National Heart, Lung, and Blood Institute, National Institutes of Health, Bethesda, MD

Abstract

Purpose—MRI-guided interventions demand high frame-rate imaging, making fast imaging techniques such as spiral imaging and echo planar imaging (EPI) appealing. In this study, we implemented a real-time distortion correction framework to enable the use of these fast acquisitions for interventional MRI.

Methods—Distortions caused by gradient waveform inaccuracies were corrected using the gradient impulse response function (GIRF), which was measured by standard equipment and saved as a calibration file on the host computer. This file was used at runtime to calculate the predicted k-space trajectories for image reconstruction. Additionally, the off-resonance reconstruction frequency was modified in real-time to interactively de-blur spiral images.

Results—Real-time distortion correction for arbitrary image orientations was achieved in phantoms and healthy human volunteers. The GIRF predicted k-space trajectories matched measured k-space trajectories closely for spiral imaging. Spiral and EPI image distortion was visibly improved using the GIRF predicted trajectories. The GIRF calibration file showed no systematic drift in 4 months and was demonstrated to correct distortions after 30 minutes of continuous scanning despite gradient heating. Interactive off-resonance reconstruction was used to sharpen anatomical boundaries during continuous imaging.

Conclusions—This real-time distortion correction framework will enable the use of these high frame-rate imaging methods for MRI-guided interventions.

Keywords

interventional; spiral; EPI; gradient impulse response; gradient calibration; off-resonance correction

INTRODUCTION

MRI-guided interventions demand real-time MRI consisting of high frame rate imaging (both image acquisition and image reconstruction), on-the-fly modification of image orientation and contrast, and low radiofrequency (RF) energy sequences when using

[*]Corresponding Author: Adrienne E Campbell-Washburn, National Institutes of Health, 9000 Rockville Pike, Building 10, Room B1D416, Bethesda MD 20892, adrienne.campbell@nih.gov, 301-402-1032.

conductive devices. Fast imaging methods such as echo planar imaging (EPI) and spiral imaging are excellent candidates to provide high frame rate and signal-to-noise ratio-efficient imaging in the interventional setting (1). Furthermore, spiral imaging and EPI are RF-efficient because they use fewer RF pulses, longer readouts and low flip angles for gradient echo readouts, potentially relieving concerns of heating in metallic devices.

Unfortunately, EPI and non-Cartesian acquisitions can be difficult to apply in the clinical setting due to the propensity for image distortion. One source of image distortion is imperfections in gradient waveforms caused by hardware (amplifier and coil characteristics, eddy current compensation and vibration induced fields). Nominal gradient waveforms prescribed in the pulse sequence are distorted when they play out in the bore, leading to distortion in the reconstructed images. This distortion can be corrected using retrospective measurements of the true gradient fields for a specified image orientation and sequence parameters (2,3). However, in the context of interactive real-time imaging, a retrospective measurement of the true gradient fields is impractical, as image orientation is constantly changing and time is critical.

Another source of image distortion for non-Cartesian imaging is blurring caused by off-resonance. Blurring can be corrected using off-resonance reconstruction, typically requiring a measured field map and/or multiple image reconstructions (4–9). Again, field map measurements or time-consuming reconstruction algorithms are impractical in an interactive real-time setting.

Recently, measurement of the impulse response has emerged as a method to characterize the gradient system (10). The gradient impulse response function (GIRF) has been used to predict the true k-space trajectories from the nominal trajectories in post-processing (10–12), and to predetermine optimal input waveforms (13).

In this study, a real-time framework is implemented using the GIRF to predict the true gradient waveforms for arbitrary image orientations, and is demonstrated for spiral imaging and EPI. In addition, an interactive off-resonance reconstruction is used to de-blur regions of interest during continuous spiral imaging. This real-time distortion correction framework will permit the use of these efficient trajectories for high frame-rate, low SAR imaging during MRI-guided interventions.

METHODS

GIRF Measurement

The GIRF was used to characterize all the imperfections in the gradient system affecting the time-evolving gradient fields. A detailed theory of GIRF measurement was provided in Vannesjo et al (10). Under the assumption that the gradient system is linear and time-invariant, a convolution of the nominal (input) gradient waveforms with the GIRF was used to predict waveforms truly played in the scanner bore.

$$o(t)=\int_{-\infty}^{\infty} i(\tau)\cdot h(t-\tau)d\tau \xleftrightarrow{FT} O(\omega)=I(\omega)\cdot H(\omega) \quad \text{Eqn 1}$$

Where i(t), o(t) and h(t) are the input, output and gradient impulse response, respectively, in the temporal domain. I(ω), O(ω), and H(ω) are the Fourier Transforms, ω represents frequency, and H(ω) is the gradient transfer function.

To measure the GIRF, the gradient system in a clinical MRI system (Aera, Siemens, Erlangen, Germany) was probed with a series of triangular waveforms (13 triangles, slew rate = 169 mT/m/s, triangle gradient amplitude = 10–31 mT/m, triangle length =120–340 μs, positive and negative polarity). The gradient system response was measured, as described in the following section, using 38 ms readouts with 9.5 μs dwell time, resulting in a frequency resolution of 26.3 Hz. Bandwidth was matched to nominal gradients prescribed in the sequence (100 kHz). The gradient transfer function was calculated by:

$$H(\omega)=\frac{\sum_j I_j^*(\omega)\cdot O_j(\omega)}{\sum_j |I_j(\omega)|^2+\sigma} \quad \text{Eqn 2}$$

where j counts the triangle number, and σ is a measure of the noise described below.

Gradient waveform measurements

The true gradient waveforms were measured in a spherical phantom (2,3). Following a slice-selective 90° pulse, the signal was measured while the test gradient played out along the same axis as the slice-selective gradient. This experiment was performed in two parallel slices and the gradient was calculated using the difference in phase evolution between the slices:

$$G(t)=\frac{1}{\gamma\cdot\Delta x}\cdot\frac{d}{dt}(\Delta\phi(t)) \quad \text{Eqn 3}$$

When measuring the triangle waveforms for GIRF calculation (O(ω)), the following parameters were used: repetition time (TR) = 7.5 s, flip angle = 90°, 4000 samples, slice thickness = 3mm, slice gap (Δx) = 33mm, receiver bandwidth = 80 Hz/Px, 32 averages, dwell time = 9.5 μs.

Reference scans without test gradients were used to determine the inherent difference in phase evolution between slices $\Delta\varphi_{ref}(t)$, which is subtracted from $\Delta\varphi(t)$:

$$G(t)=\frac{1}{\gamma\cdot\Delta x}\cdot\frac{d}{dt}(\Delta\phi(t)-\Delta\phi_{ref}(t)) \quad \text{Eqn 4}$$

The standard deviation of the residuals between this reference phase, $\varphi_{ref}(t)$, and a linear fit was used as an estimate of the measurement noise (σ, Eqn 2) to filter the GIRF.

The GIRF was calculated in the Siemens Image Calculation Environment (ICE, Siemens Medical Solutions, Erlangen, Germany) and saved as a file on the host computer. The GIRF was measured eight times during 4 months to assess the drift in the gradient system.

Real-time GIRF trajectory prediction

The most recent GIRF file saved on the host computer was convolved with the nominal gradient waveforms in physical (x, y, z) coordinates to calculate predicted k-space trajectories using the Siemens ICE. For implementation, the calibration file contained the Fourier Transform of the GIRF (gradient transfer function) and the convolution was performed using multiplication in the frequency domain. The gradient waveforms were resampled and shifted in time to match the readout (14), such that the trajectories match the exact timing of acquired data points. The waveforms were rotated back to logical coordinates (frequency, phase) for arbitrary oblique slices. The data and the predicted k-space trajectories were exported in real-time from ICE in ISMRMRD format (http://ismrmrd.github.io) to the Gadgetron open source reconstruction software (http://gadgetron.github.io) (15) running on an external workstation. Images were reconstructed by data regridding according to the GIRF predicted trajectories and images were piped back to the MRI host computer for real-time display.

For EPI, the true gradient waveforms for the entire duration of the echo train were predicted using convolution with the GIRF, then relevant time periods during signal acquisition were selected to match data points. EPI reference scans were not used during reconstruction with GIRF predicted trajectories.

Off-resonance reconstruction

For spiral imaging, reconstruction frequency (f) was implemented as an interactive parameter, which was modified during imaging to de-blur an area-of-interest in real-time. Each data point was multiplied by phase term [$exp(-i2\pi ft)$] before export to the Gadgetron.

A schematic diagram demonstrating the real time trajectory prediction and off-resonance reconstruction is shown in Figure 1.

Phantom experiments

Imaging was performed on a 1.5T MRI scanner (Aera, Siemens, Erlangen, Germany). Variable density spiral trajectories were calculated using freely available software (http://mrsrl.stanford.edu/~brian/vdspiral/).

For spiral imaging, nominal and GIRF predicted trajectories were compared to true trajectories measured in a spherical phantom using the phase evolution in two parallel slices (2,3). Images from a structural phantom were reconstructed using: 1) nominal trajectories, 2) GIRF predicted trajectories, and 3) measured trajectories (Eqn 4). Parameters for spiral imaging were as follows: 8 interleaves (echo time [TE]/TR = 0.86/8.6 ms) or 4 interleaves (TE/TR = 0.86/15.51 ms), flip angle = 10°, thickness = 5mm, field of view (FOV) = 300 mm, matrix = 128 × 128, bandwidth (BW) = 1000 Hz/Px.

For EPI, nominal and GIRF predicted trajectories were compared. Images of a structural phantom were reconstructed using: 1) a standard 2D Fourier Transform of the raw data, 2) the default vendor-provided reconstruction with biopolar reference scans, and 3) regridding data according to the GIRF predicted trajectories. EPI parameters were as follows: echo train length = 8, TE/TR = 4.86/8.96 ms, flip angle = 15°, thickness = 5mm, FOV = 300 mm,

matrix = 128 × 128, BW = 1953 Hz/Px. Spiral and EPI images were both compared to a standard Cartesian gradient echo image in the same orientation (TE/TR = 10 ms/100 ms, FOV = 300 mm, matrix = 128 × 128, thickness = 5mm, flip angle = 15°).

Busch et al (16) demonstrated changes in the GIRF caused by temperature increases in the gradient system. In order to assess the quality of the distortion correction afforded from the previously measured GIRF during the long periods of continuous scanning relevant to the interventional MRI setting, 30 minutes of continuous spiral imaging was performed (16 interleaves, TE/TR = 0.86/5.16 ms, flip angle = 10°, thickness = 5mm, FOV = 300 mm, matrix = 128 × 128, BW = 1000 Hz/Px). The first and final frames were compared to assess image distortion. Off-resonance reconstruction was tested in a phantom containing gadolinium doped water (0.2mM solution) and vegetable oil.

In vivo imaging

In vivo imaging was performed in a healthy human volunteer using a protocol approved by the Institutional Review Board and with written informed consent from the subject. Spiral imaging was performed with either 8 interleaves (TE/TR = 0.78/9.6 ms) or 16 interleaves (TE/TR = 0.78/7.5 ms) and the following parameters: flip angle = 10°, thickness = 8mm, FOV = 420 mm, matrix = 128 × 128, BW = 700 Hz/Px, 24 receive channels. EPI parameters were as follows: echo train length = 8, TE/TR = 4.2/7.9ms, flip angle = 15°, thickness = 8 mm, FOV = 420 mm, matrix = 128 × 128, BW = 1953 Hz/Px. Real-time GIRF trajectory prediction was assessed and interactive modification of the reconstruction frequency was demonstrated in the volunteer.

RESULTS

Measured GIRF

The gradient impulse response function was measured with a frequency resolution of 26 Hz, and BW of 100 kHz. The GIRF exhibited low pass behavior in all axes with peaks corresponding to mechanical resonances of the gradient coils (Figure 2). No systematic change was observed during repeated measurements over 4 months, and relative changes from the first measurement were less than 2% between ±10 kHz in all axes. This indicates that measurement of the GIRF approximately once every month during standard scanning calibration will be sufficient.

Phantom experiments

Figure 3 shows the nominal, measured and GIRF predicted spiral k-space trajectories and corresponding images for an oblique slice through a structural phantom. The GIRF predicted trajectories accurately reflected true gradient behavior, and thus corresponded well to the measured trajectories. Error accumulation results from subtle timing differences between the trajectories (Figure 3b). For a 4 interleave spiral acquisition, the root mean squared error (RMSE) between the measured and GIRF predicted trajectories was reduced compared to the RMSE between measured and nominal trajectories for axial/coronal/sagittal orientations ($RMSE_{nominal}$ = 0.0330 ± 0.0010 m^{-1} vs $RMSE_{predicted}$ = 0.0109 ± 0.0003 m^{-1}) and three arbitrary oblique orientations ($RMSE_{nominal}$ = 0.0329 ± 0.0006 m^{-1} vs $RMSE_{predicted}$ =

$0.0097 \pm 0.0020\ m^{-1}$). Reconstruction using the nominal trajectories results in a visible image rotation and signal halo, whereas this distortion is eliminated when the measured or GIRF predicted trajectories are used for reconstruction.

Similarly, for an oblique echo planar image, reconstruction using the GIRF predicted trajectories removed the distortion (ghosting outside object and signal displacement within object) visible in the simple Fourier Transformed image (Figure 4). EPI bipolar reference lines were not used for reconstruction from the GIRF predicted trajectory. GIRF predicted trajectories generated images that were similar or better than online reconstruction employing bipolar reference lines.

Following 30 minutes of continuous scanning, the GIRF calibration file still adequately corrected the image distortions caused by trajectory inaccuracy, namely image rotation and signal halo in spiral images (Figure 5). Increased image blurring is observed after 30 minutes of scanning for both the nominal and GIRF predicted trajectories.

Using a phantom containing vegetable oil and doped water, the off-resonance reconstruction parameter was modified to de-blur vegetable oil at the expense of water blurring. Blurring manifested as a signal pileup inside the object plus a signal smearing. A demonstration of interactive de-blurring is available in Supporting Video S1.

In vivo imaging

A frame rate of 13.0 frames/s (8 interleaves) or 8.3 frames/s (16 interleaves) was achieved using spiral imaging and 7.9 frames/s using EPI. The real time calculation of GIRF predicted trajectories for reconstruction was successfully applied to improve in vivo spiral images (Figure 6) and echo planar images (Figure 7). Supporting Video S2 shows the GIRF trajectory prediction being turned on/off in real-time to correct spiral images three different image orientations (16 interleave imaging protocol). In this video, the removal of the signal halo and image rotation using GIRF predicted trajectories is clear.

The off-resonance reconstruction frequency was used to regionally de-blur images in vivo (Figure 8), in order to improve vessel boundary delineation and reduce signal pileup caused by off-resonance at epicardial fat. These images were acquired with local shimming around the heart and different off-resonance frequencies are needed for local deblurring in different imaging planes and areas-of-interest. Interactive adjustment of the reconstruction frequency is demonstrated in Supporting Video S3.

DISCUSSION

We have demonstrated a real-time framework for distortion correction of spiral and echo planar images. This framework involved an occasional measurement of the gradient impulse response function that is calculated in the scanner reconstruction environment and stored as a calibration file on the host computer. At run-time, the GIRF is used to predict the true k-space trajectories for use during reconstruction, and an interactive modification of the reconstruction frequency is used for local de-blurring of spiral images. This real-time framework for distortion correction is orientation independent and may enable the use of

spiral imaging and EPI for high frame-rate and RF-efficient imaging during MRI-guided interventions. Furthermore, this real-time framework could be extended to apply to any arbitrary k-space trajectory.

One of the primary motivations for moving to non-Cartesian imaging or EPI for MRI-guided interventions is the high frame rate. Currently, using Cartesian bSSFP, frame rates up to 7 frames/second (with undersampling and parallel imaging factor 4) are used for MRI-guided catheterizations (17). This slow frame rate is considered a weakness of MRI-guidance compared to traditional X-Ray guidance which achieves up to 15–30 frames/s. Here, we were able to achieve 13.0 frames/s with spiral imaging (8 interleave protocol), and 7.9 frames/s using EPI, which could be improved using parallel imaging. An additional benefit of non-Cartesian imaging and EPI is the RF-efficiency. These acquisition schemes employ fewer RF pulses, longer readouts between pulses and lower flip angles (for gradient echo imaging), and thus reduce the potential for RF-induced heating on devices (18). The orientation-independence of this correction is important in the interventional MRI environment, since slice geometry is constantly changing according to the needs of the procedure. The RMSE between measured and GIRF predicted trajectories was the same for both orthogonal and oblique slices, indicating that interaction between two gradients playing simultaneously was minimal. In a similar study, an orientation independent correction for high order eddy currents in EPI, was implemented using a one-time calibration step (19).

Here, we did not employ a field camera for GIRF measurement, as has been used before (10,20). Instead, we used standard equipment to measure triangular gradient waveforms and estimate the GIRF. Liu et al previously demonstrated the accurate calculation of the GIRF using standard equipment (11). We measured a GIRF with a frequency resolution of 26 Hz, compared to 14.7 Hz reported with a field camera (10). A small DC component was present in our measured GIRFs presumably caused by long time-constant Eddy currents. The GIRF measurement took ~12 hours for all three gradient axes [TR = 7.5 s × 2 slices x (26 gradient waveforms + 2 reference scans) × 32 averages = 3.73 hours per gradient axis], and was run overnight with online GIRF calculation, such that new GIRF files were saved when scanning began the following morning. Gradient heating is not a concern during this calibration due to the low gradient duty cycle (TR = 7.5 s). We demonstrated here that there was no systematic drift and very small change in the GIRF within 4 months of scanning. Therefore, we would recommend measuring the GIRF approximately every month, in order to maintain an up-to-date measurement.

Previous studies have used the GIRF to predict k-space trajectories and correct image distortion as an offline post-processing step (10–12). Our approach differs from these previous studies because all processing is performed online in the reconstruction software, and the corrections take effect during real-time imaging. There are other methods to achieve real-time distortion correction. In sites with access to the equipment, real-time field monitoring could be employed for trajectory calculation (21). Alternatively, The GIRF could be used to calculate the input waveform needed to produce the ideal waveform in the scanner bore, and thus, corrected waveforms could be prescribed in the pulse sequence (13).

The interactive adjustment of the off-resonance reconstruction frequency for spiral imaging is a powerful tool in the interventional MRI setting. During the course of an MRI-guided cardiovascular intervention, interventionists are navigating their instruments from a peripheral access site, and may need to image vasculature inferior to the heart, vasculature superior to the heart, the chambers of the heart and the chest wall, all within a single procedure without pausing continuous interactive scanning. Therefore, it is reasonable to assume that in some image planes there will be noticeable off-resonance blurring due to locally shimming or intrinsic sources such as fat. Thus, the ability to adapt to local off-resonance on-the-fly is essential for the application of spiral imaging to MRI-guided interventions.

In the future, we will also apply this real-time framework more generally to diagnostic MRI scanning susceptible to image distortion and to other k-space trajectories. The ability to predict true k-space trajectories online on the MRI scanner, will remove additional post-processing steps.

In conclusion, a real-time framework has been presented to remove image distortion for EPI and non-Cartesian imaging using the gradient impulse response function measured with standard equipment. This framework may enable the reliable use of non-Cartesian imaging and EPI to achieve high frame-rates within the context of MRI-guided interventions.

Supplementary Material

Refer to Web version on PubMed Central for supplementary material.

Acknowledgments

This work was supported by the National Heart, Lung, and Blood Institute Division of Intramural Research (Z01-HL006039-01, Z01-HL005062-08).

References

1. Terashima M, Hyon M, de la Pena-Almaguer E, Yang PC, Hu BS, Nayak KS, Pauly JM, McConnell MV. High-resolution real-time spiral MRI for guiding vascular interventions in a rabbit model at 1. 5 T. J Magn Reson Imaging. 2005; 22(5):687–690. [PubMed: 16217745]
2. Duyn JH, Yang Y, Frank JA, van der Veen JW. Simple correction method for k-space trajectory deviations in MRI. J Magn Reson. 1998; 132(1):150–153. [PubMed: 9615415]
3. Zhang Y, Hetherington HP, Stokely EM, Mason GF, Twieg DB. A novel k-space trajectory measurement technique. Magn Reson Med. 1998; 39(6):999–1004. [PubMed: 9621924]
4. Noll DC, Meyer CH, Pauly JM, Nishimura DG, Macovski A. A homogeneity correction method for magnetic resonance imaging with time-varying gradients. IEEE Trans Med Imaging. 1991; 10(4): 629–637. [PubMed: 18222870]
5. Noll DC, Pauly JM, Meyer CH, Nishimura DG, Macovski A. Deblurring for non-2D Fourier transform magnetic resonance imaging. Magn Reson Med. 1992; 25(2):319–333. [PubMed: 1614315]
6. Man LC, Pauly JM, Macovski A. Multifrequency interpolation for fast off-resonance correction. Magn Reson Med. 1997; 37(5):785–792. [PubMed: 9126954]
7. Man LC, Pauly JM, Macovski A. Improved automatic off-resonance correction without a field map in spiral imaging. Magn Reson Med. 1997; 37(6):906–913. [PubMed: 9178243]

8. Irarrazabal P, Meyer CH, Nishimura DG, Macovski A. Inhomogeneity correction using an estimated linear field map. Magn Reson Med. 1996; 35(2):278–282. [PubMed: 8622593]
9. Chen W, Meyer CH. Semiautomatic off-resonance correction in spiral imaging. Magn Reson Med. 2008; 59(5):1212–1219. [PubMed: 18429033]
10. Vannesjo SJ, Haeberlin M, Kasper L, Pavan M, Wilm BJ, Barmet C, Pruessmann KP. Gradient system characterization by impulse response measurements with a dynamic field camera. Magn Reson Med. 2013; 69(2):583–593. [PubMed: 22499483]
11. Liu H, Matson GB. Accurate Measurement of Magnetic Resonance Imaging Gradient Characteristics. Materials (Basel). 2014; 7(1):1–15. [PubMed: 25343017]
12. Addy NO, Wu HH, Nishimura DG. Simple method for MR gradient system characterization and k-space trajectory estimation. Magn Reson Med. 2012; 68(1):120–129. [PubMed: 22189904]
13. Goora FG, Colpitts BG, Balcom BJ. Arbitrary magnetic field gradient waveform correction using an impulse response based pre-equalization technique. J Magn Reson. 2014; 238:70–76. [PubMed: 24316188]
14. Speier, P.; Trauterin, F. A Calibration for Radial Imaging with Large Inplane Shifts. Proceedings of the International Society for Magnetic Resonance in Medicine; Miami, Florida, USA. 2005. p. 2295
15. Hansen MS, Sørensen TS. Gadgetron: an open source framework for medical image reconstruction. Magn Reson Med. 2013; 69(6):1768–1776. [PubMed: 22791598]
16. Busch J, Vannesjo SJ, Barmet C, Pruessmann KP, Kozerke S. Analysis of temperature dependence of background phase errors in phase-contrast cardiovascular magnetic resonance. J Cardiovasc Magn Reson. 2014; 16:97. [PubMed: 25497004]
17. Ratnayaka K, Faranesh AZ, Hansen MS, Stine AM, Halabi M, Barbash IM, Schenke WH, Wright VJ, Grant LP, Kellman P, Kocaturk O, Lederman RJ. Real-time MRI-guided right heart catheterization in adults using passive catheters. Eur Heart J. 2013; 34(5):380–389. [PubMed: 22855740]
18. Konings MK, Bartels LW, Smits HF, Bakker CJ. Heating around intravascular guidewires by resonating RF waves. J Magn Reson Imaging. 2000; 12(1):79–85. [PubMed: 10931567]
19. Xu D, Maier JK, King KF, Collick BD, Wu G, Peters RD, Hinks RS. Prospective and retrospective high order eddy current mitigation for diffusion weighted echo planar imaging. Magn Reson Med. 2013; 70(5):1293–1305. [PubMed: 23325564]
20. Vannesjo SJ, Dietrich BE, Pavan M, Brunner DO, Wilm BJ, Barmet C, Pruessmann KP. Field camera measurements of gradient and shim impulse responses using frequency sweeps. Magn Reson Med. 2014; 72(2):570–583. [PubMed: 24105800]
21. Kasper L, Bollmann S, Vannesjo SJ, Gross S, Haeberlin M, Dietrich BE, Pruessmann KP. Monitoring, analysis, and correction of magnetic field fluctuations in echo planar imaging time series. Magn Reson Med. 2014

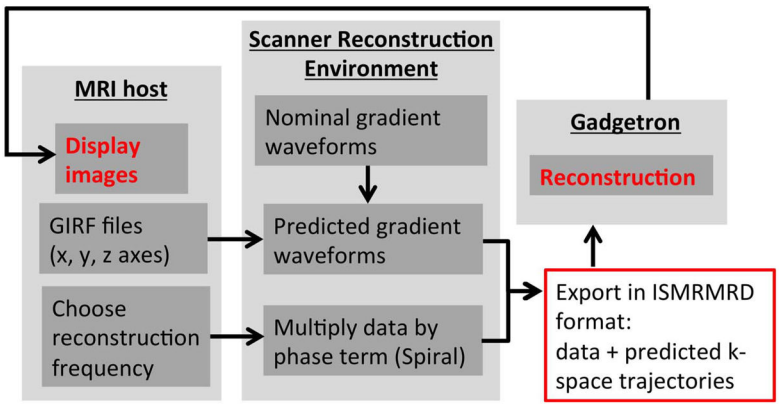

Figure 1.

Real time framework for distortion correction using most recent GIRF calibration file saved on the host computer to predict trajectories in the Siemens Image Calculation Environment. For spiral imaging, reconstruction frequency is modified on-the-fly. Data is sent with predicted trajectories in ISMRMRD format to the Gadgetron for image reconstruction.

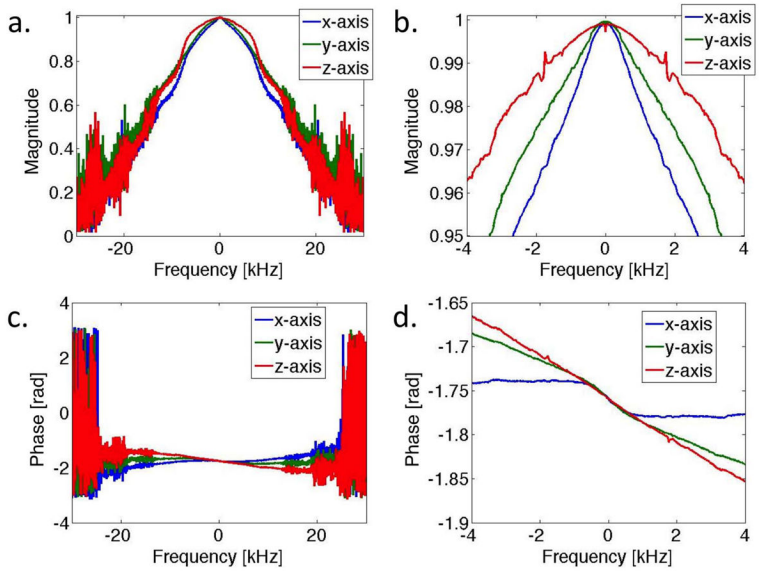

Figure 2.

Magnitude (a,b) and phase (c,d) of the GIRF in the frequency domain (gradient transfer function) measured in all three gradient axes. A maximum frequency range of ±30kHz is displayed (a,c), as well as a narrower range of ±4kHz (b,d).

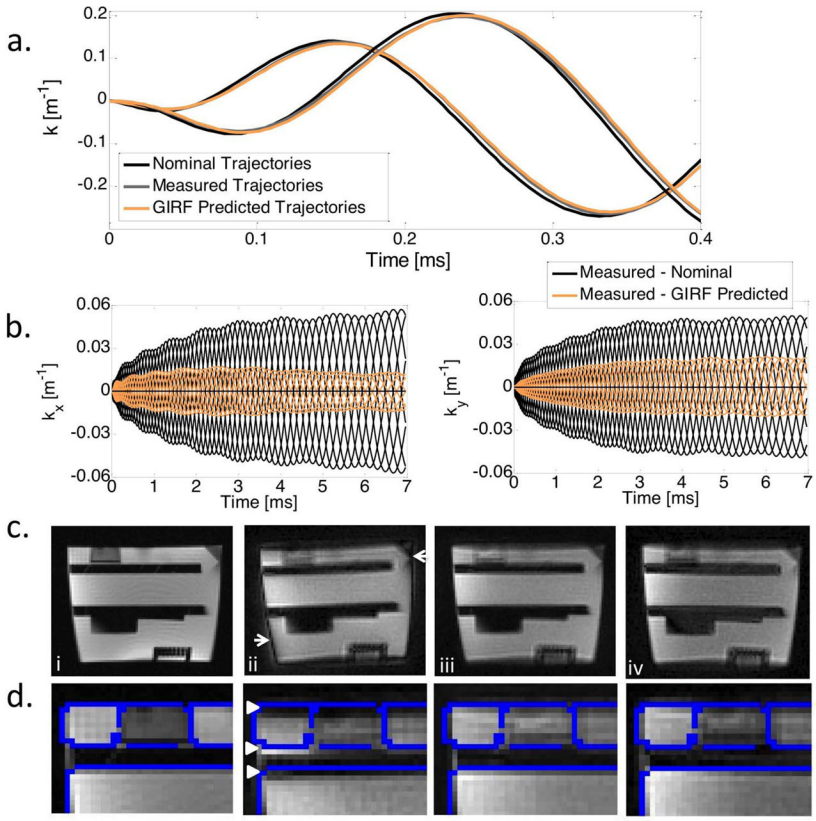

Figure 3.

a) Nominal, measured and GIRF predicted spiral k_x and k_y trajectories (first 0.4 ms) for a double oblique imaging slice. b) Difference between measured trajectories and nominal or GIRF predicted trajectories for the entire trajectory duration for all 8 interleaves. c) Comparison of images between a Cartesian gradient echo image (i), and spiral images reconstructed using nominal trajectories (ii), measured trajectories (iii) and GIRF predicted trajectories (iv), with a zoomed-in image of top left corner (d). Edges of the Cartesian gradient echo image are overlaid in blue (d) to emphasize image alignment. Reconstruction using nominal trajectories shows a clear signal halo (c, arrows) and rotation (d, arrow heads), whereas reconstruction using GIRF predicted trajectories (iv) eliminates these image distortions.

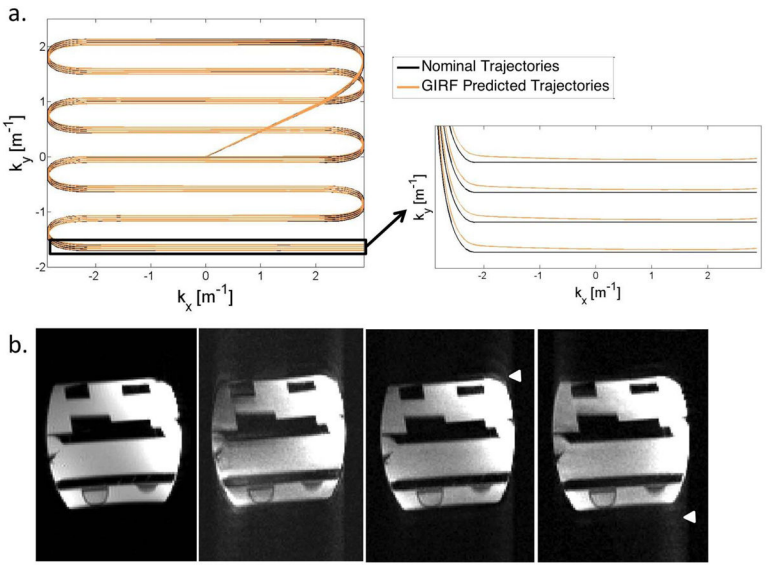

Figure 4.

A comparison of nominal and GIRF predicted k-space trajectories for the first 4 echo trains of an EPI acquisition (a), with zoomed-in plot showing the final echoes of the trains to demonstrate trajectory deviation. b) Comparison of standard Cartesian gradient echo imaging (i), EPI image reconstructed using: simple 2D Fourier Transform (ii), the default vendor-provided algorithm (with bipolar reference lines) (iii) and GIRF predicted trajectories (iv). Simple 2D Fourier Transform reconstruction shows significant image distortion in the form of ghosting outside of the object and signal displacement within the object. An improvement in image distortion is obtained with GIRF predicted trajectories. Arrowheads show region of residual distortion in corrected images.

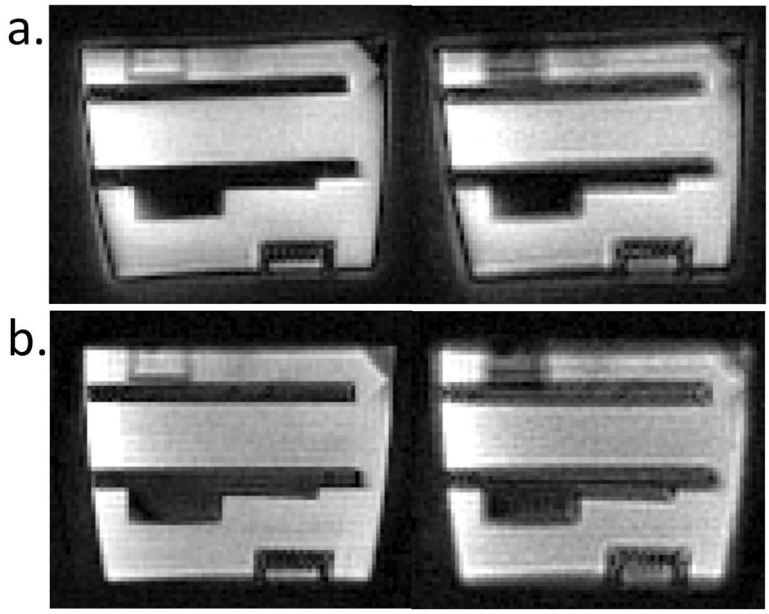

Figure 5.
Side-by-side comparison of the first (left) and final (right) frame during 30 minutes of continuous spiral imaging using reconstruction with the nominal trajectories (a) and GIRF predicted trajectories (b).

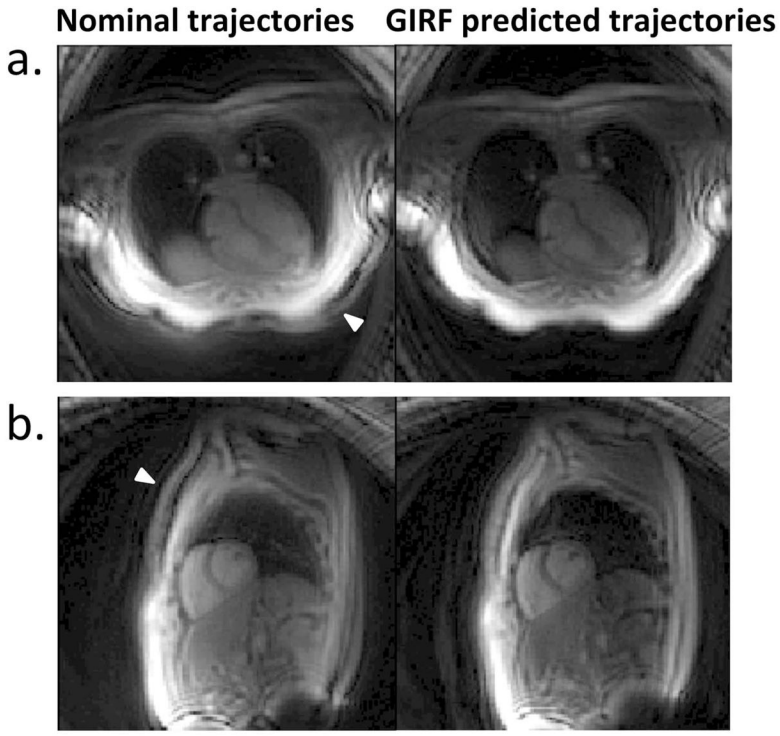

Figure 6.

In vivo spiral images (8 interleave protocol) depicting a four chamber view (a) and short axis view (b). The same frame is reconstructed using nominal trajectories (left) and GIRF predicted trajectories (right). The signal halo distortion (arrowheads) is removed and the image quality is improved using the GIRF predicted trajectories.

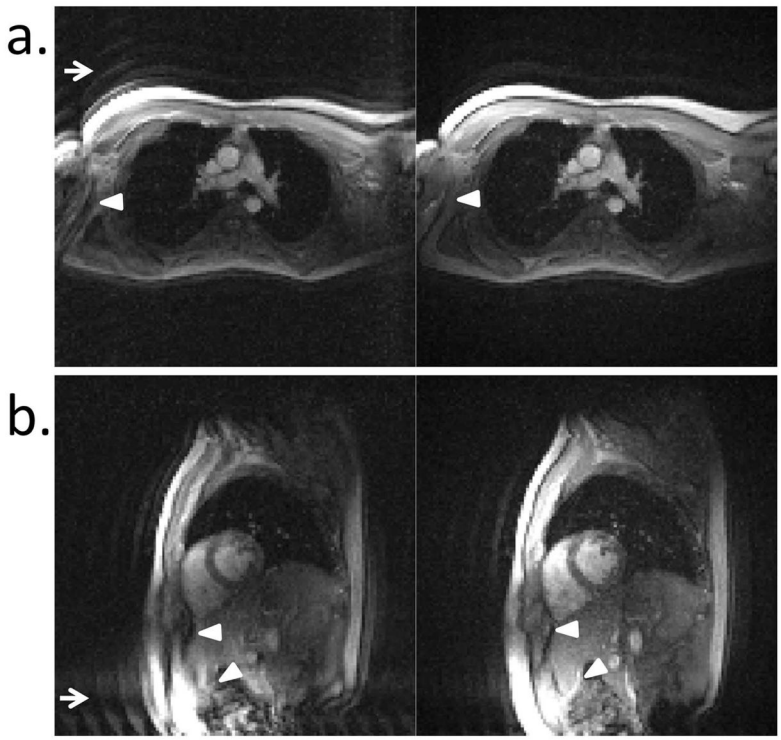

Figure 7.

In vivo echo planar images depicting the pulmonary artery branch (a) and a short axis view (b). The same frame is reconstructed using 2D Fourier Transform (left) and GIRF predicted trajectories (right). The signal ghosting (arrows) and signal distortion within the object (arrowheads) are improved using the GIRF predicted trajectories.

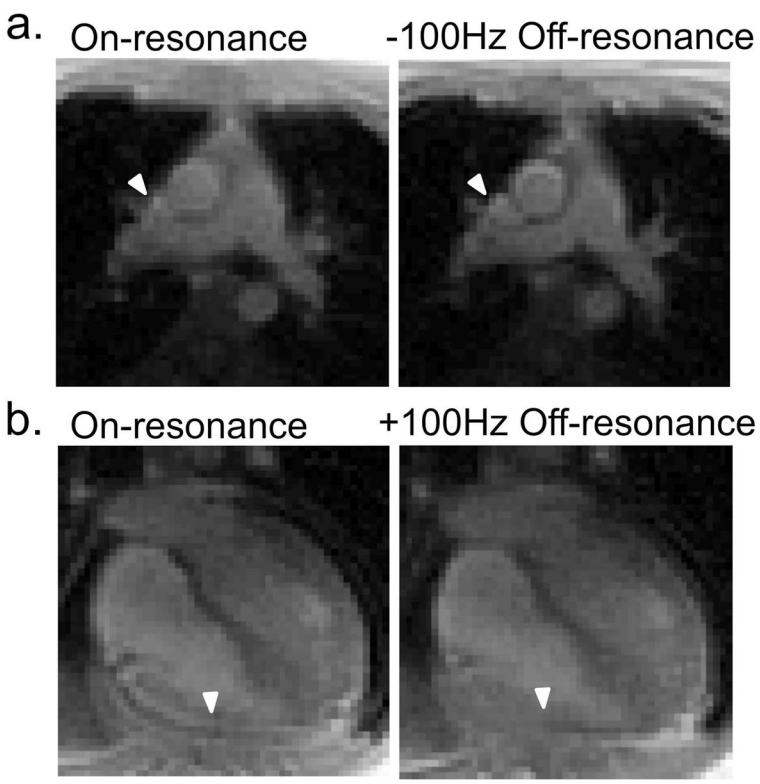

Figure 8.

Off resonance reconstruction used to locally deblur spiral images (16 interleave protocol) for a view of the pulmonary artery branch (a) and a four-chamber view (b). Arrowheads depict the sharpening of the vessel boundary (a) and removal of signal pileup caused by epicardial fat off-resonance at the right ventricle wall (b), using reconstruction at −100 Hz and +100Hz off-resonance, respectively. A shim volume localized around the heart was used during imaging.